Chapter 6

Laterally Inhomogeneous Au Intercalation in Epitaxial Graphene on SiC(0 0 0 1): A Multimethod Electron Microscopy Study

Claire Mathieu, Tevfik Onur Menteş, Emiliano Pallecchi, Andrea Locatelli, Gilles Patriarche, Rachid Belkhou and Abdelkarim Ouerghi

Additional information is available at the end of the chapter

http://dx.doi.org/10.5772/64076

Abstract

Epitaxial graphene is of particular interest because of its tunable electronic structure. One important approach to tune the electronic properties of graphene relays on intercalating atomic species between graphene and the topmost silicon carbide layer. Here, we investigated the morphology and electronic structure of gold-intercalated epitaxial graphene using a multitechnique approach combining spectroscopic photoemission low-energy electron microscopy (SPELEEM) for chemical and structural characterization at mesoscopic length scale and with transmission electron microscopy (STEM) at the atomic level. Deposition of gold on ex situ prepared graphene on SiC(0 0 0 1) results in the partial intercalation of Au adatoms under graphene, with the formation of a buffer layer of variable thickness. Gold has also shown to aggregate in nanometer-sized clusters lying on top of the same graphene film. X-ray photo-emission electron microscopy measurements indicate that Au induces only small changes in the doping of the graphene layer, which does not develop a quasi free-standing behavior.

Keywords: graphene, electronic properties, ARPES, LEEM/LEED, STEM

1. Introduction

Graphene is a single layer of carbon atoms arranged in a hexagonal lattice. It is one of the few structures that are stable in two dimensions as a free-standing crystal [1, 2]. Its extraordinary properties, such as unconventional two-dimensional (2D) electron gas, high carrier mobility, half-integer quantum Hall effect at room temperature, and spin transport [1], have made graphene a very promising candidate for the design of the new generation of devices, such as ultrafast electronic circuits and photodetectors. Despite significant progress in its synthesis, the development of production methods warranting fine control over film morphology and thickness, which are both crucial to determine its electronic properties, remains a considerable challenge.

Epitaxial graphene layers on silicon carbide (SiC) have been extensively studied due to their potential for large-scale production with a high crystalline quality [3, 4]. It is now well established that, in this system, the interaction between the graphene and its supporting substrate (SiC) can affect considerably the electronic properties of graphene. Indeed, it is known that the first carbon layer onto a SiC substrate is covalently bonded to the Si atoms of the substrate, and this "buffer layer" does not display graphitic electronic properties [5–8]. Moreover, the remaining unsaturated Si dangling bonds, at the buffer layer/SiC interface, induce a high intrinsic n-doping in graphene, which degrades the carrier mobility. These drawbacks pose a major obstacle to the integration of graphene/SiC in future electronic devices. A solution to this problem is provided by the passivation of the Si dangling bonds using dopants and/or decoupling the graphene layer from the SiC substrate. Recently, decoupling of graphene has been achieved by depositing molecules [9, 10] or atomic layers of Bi [11], Ge [12], F [13], and Li [14, 15]. Furthermore, Riedl et al. [16] have shown that hydrogen intercalation can induce such desired decoupling. More recently, it was demonstrated that the oxygen can partially decouple the buffer layer from the substrate and reduce the intrinsic electron doping [17]. Moreover, the intercalation of metal clusters or molecules between the graphene layers may serve to functionalize graphene.

Numerous studies have been performed to understand the intercalation of transition metals [18–20]. The study by Gierz et al. [21] claimed that the strongly interacting first carbon layer was decoupled from the SiC(0 0 0 1) substrate via gold intercalation. The shift of Dirac points due to gold intercalation was then theoretically studied by Chuang et al. [22]. A similar study performed by Premlal et al. [23], using scanning tunneling microscopy and spectroscopy (STM/STS), concluded that the intercalated gold cluster displays a new surface reconstruction and induces a possible hole-doping effect. Nonetheless, further investigations are needed to better clarify the effects on the electronic structure of graphene induced by intercalated Au.

In this chapter, we discuss the properties of Au-intercalated epitaxial graphene grown on 6H-SiC(0 0 0 1). Low-energy electron diffraction (LEED), low-energy electron microscopy (LEEM), transmission electron microscopy (TEM), X-ray photoemission electron microscopy (XPEEM), microspot angle-resolved photoemission spectroscopy (μ-ARPES), and micro-Raman spectroscopy allowed us to study the structural and electronic properties of epitaxial graphene on SiC. In particular, we focused on the effect of Au adsorption on the local morphology, structure,

http://dx.doi.org/10.5772/64076

and electronic properties of few layers graphene on SiC(0 0 0 1); as it will be shown, our work provides also information about the local distribution of Au at the interface.

2. Experimental details

The structural and electronic properties of the graphene/SiC interface were characterized using the SPELEEM III (Elmitec GmbH) microscope operating at the Nanospectroscopy beamline of the Elettra storage ring in Trieste (Italy). This instrument combines LEEM and energy-filtered XPEEM imaging with μLEED and μARPES. The μ-spot diffraction data are typically collected from areas of diameter as small as 2 μm. Such analytical methods are well-established tools for characterizing the local morphology, thickness, corrugation, and electronic structure of single layer graphene films [24, 25].

Semi-insulating on-axis SiC(0 0 0 1) substrates were used in this study. After polishing, the samples were exposed to hydrogen etching at 1600°C in order to remove surface defects. Graphene growth was carried out by annealing the substrates at 1300–1400°C under argon and silicon fluxes. This method favors the formation of large and homogeneous domains [26, 27]. During the graphitization process, the argon partial pressure was kept below $P = 2 \times 10^{-5}$ Torr. The samples were then cooled to the room temperature and transferred ex situ to the microscopes used in these studies.

Before the measurements, the graphene samples were annealed at 600°C for 30 min in ultra-high vacuum, in order to reduce the contamination consequent to atmosphere exposure. The Au incorporation process was carried out using a post-growth deposition method. The samples were then further annealed at 800°C for 20 min in order to favor migration of gold.

In order to vary the amount of buffer layer on the surface prepared as above, we studied two samples grown under the same conditions but with different level of graphitization. As shown in the next section, sample 1 (S1) is at a later stage of graphitization in comparison with sample 2 (S2). S1 is mainly covered by 1 ML graphene, with small areas that present the characteristic of the buffer layer or bilayer graphene. On the other side, S2 presents mainly one and two graphene layers. Both samples were fully characterized by means of LEEM, μARPES, and μLEED, before and after Au deposition, respectively. Post-growth Au deposition on previously characterized graphene allows unraveling the effect of gold on the graphene layers. The Au 4f, Si 2p, and C 1s core-level images were recorded using two photon energies ($h\nu$ = 200 and 360 eV) to tune the surface sensitivity. They were calibrated using the Au 4f7/2 component.

The TEM thin foil was prepared by focused ion beam (FIB). The surface was protected by an amorphous layer carbon deposited before the FIB process. The thin foils were prepared following the <1 1 –2 0> zone axis of the SiC substrate. We used a TEM/STEM microscope Jeol 2200FS working at 200 keV equipped with a spherical aberration (Cs) corrector on the STEM probe. The probe current was 50 pA with a probe size of 0.1 nm (FWHM). The convergence half-angle for the probe was 30 mrad, and the detection half-angles for the HAADF images were, respectively, 100 mrad (inner) and 170 mrad (outer).

3. Results and discussion

3.1. Growth of graphene on SiC(0 0 0 1)

We first address the structural properties of graphene, which was studied by low-energy electron diffraction. The typical LEED of the graphene sample can be seen in **Figure 1a**. The LEED pattern demonstrates that the graphene layer is well ordered and aligned with respect to the substrate, such that the basal plane unit vectors of graphene and SiC subtend an angle of 30°. The smallest hexagon is the result of a $(6\sqrt{3} \times 6\sqrt{3})R \times 30°$ reconstruction of the interfacial layer, as are the spots lying just inside the graphene pattern.

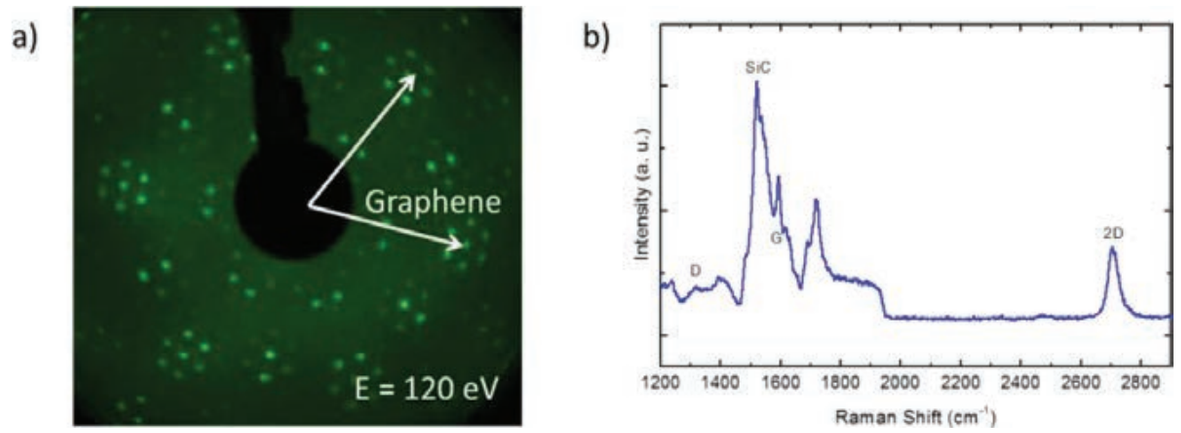

Figure 1. (a) Typical LEED image of graphene on SiC(0 0 0 1) and (b) typical micro-Raman spectra of the graphene monolayer. Contributions at the G and 2D bands are observed, together with a very low signal at the defect band D.

We further characterized our graphene by Raman spectroscopy, in **Figure 1b**, we present a typical Raman spectrum, which presents the typical features of high-quality epitaxial monolayer graphene. Graphene contributions were identified by three main structures: (i) the D band at 1350 cm^{-1}, (ii) the G band (symmetric E2g phonon mode) at 1592 cm^{-1}, and (iii) the 2D band at 2704 cm^{-1}. For both samples, the D band, which corresponds to disorder, was weak in comparison with the G and 2D bands (double resonant electron-phonon process). The low intensity of this peak showed that there was only a small number of defect/disorder in the graphene structure. This was an indication of the high quality of the epitaxial graphene produced.

3.2. Au intercalation in epitaxial graphene on SiC(0 0 0 1)

The Au incorporation process was carried out using a post-growth deposition method. Au was deposited at a temperature of 890°C, at a rate of 10 min/layer. A total coverage of 2 ML (1 ML) was deposited on sample S1 (S2). The samples were then further annealed at 800°C for 20 min in order to favor migration of gold. We now discuss the results of LEEM, μARPES, and μLEED, characterization of both samples, before and after Au deposition.

http://dx.doi.org/10.5772/64076

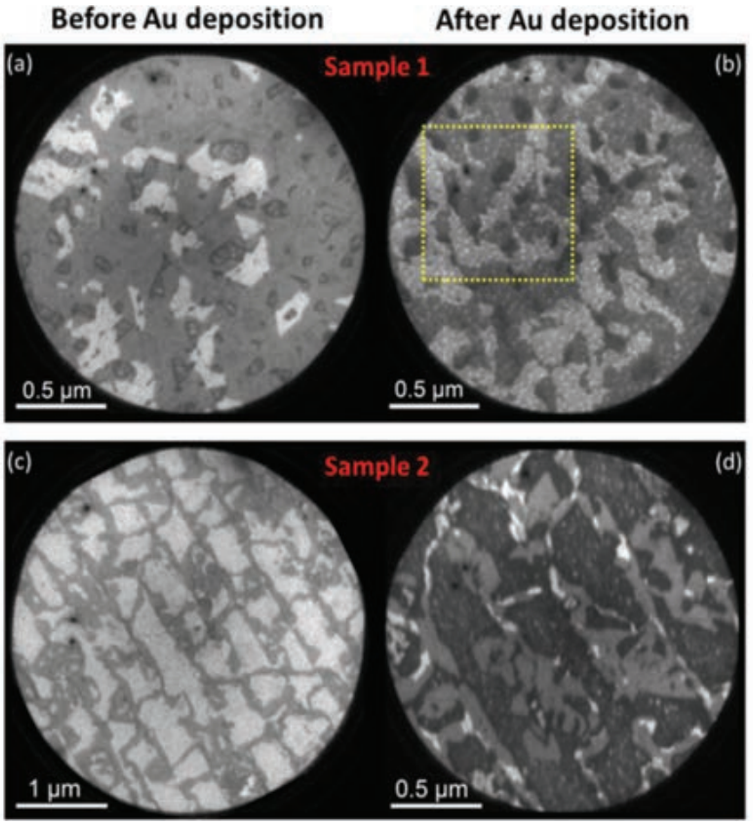

Figure 2. LEEM image of a graphene/SiC(0 0 0 1) surface, before (left) and after (right) Au deposition, with an electron beam energy of 3.90 eV. The images for the sample 1 (2) are presented at the top (bottom) of the image.

Figure 2a–d presents LEEM images obtained on the two samples before and after Au deposition. The image contrast arises from the thickness dependent reflectivity of the film. Recent quantum mechanical calculations of the IV reflectivity of graphene allow precise quantification of the graphene thickness on SiC, which vary considerably depending on the presence of buffer layers [28]. Measurement of the low energy electron reflectivity (not shown) of sample S1 before Au deposition (**Figure 1a**) has allowed us identifying the predominant presence of 1 monolayer (neutral gray regions) of graphene, accompanied with a small amount of the buffer layer (dark gray) and graphene bilayer (white contrast). After the deposition of Au (**Figure 2b**), the three regions exhibit the same contrast, suggesting that the overall thickness distribution of the sample was preserved by the Au deposition.

A notable difference between LEEM images acquired before and after Au deposition is the presence of small dots which are uniformly distributed over both single- and bilayers graphene. These structures have a maximum size of few tens of nanometers, with several of them close to (or below) the lateral resolution of our LEEM microscope. We interpret the dots as due to three-dimensional gold islands, as none of these features were observed on the sample before Au deposition. We had repeated the Au experiment on the second sample S2, with less Au (1 ML instead of 2 ML), on which the graphitization was incomplete. Indeed, the reflectivity curves confirm that the substrate was only partially covered by one and two monolayers of graphene. The rather large light gray contrast areas in **Figure 1c** are attributed to the buffer

layer, thanks to the analysis of the reflectivity curves, extracted from these areas. The corresponding image recorded after Au deposition shows that the nanoclusters are once again observed over the entire field of view. The lower concentration can be explained by the total coverage of 1 ML of gold in comparison with 2 ML Au on S1. This set of images demonstrates that the clusters nucleate also over the buffer layer, as well as on the one and two graphene MLs.

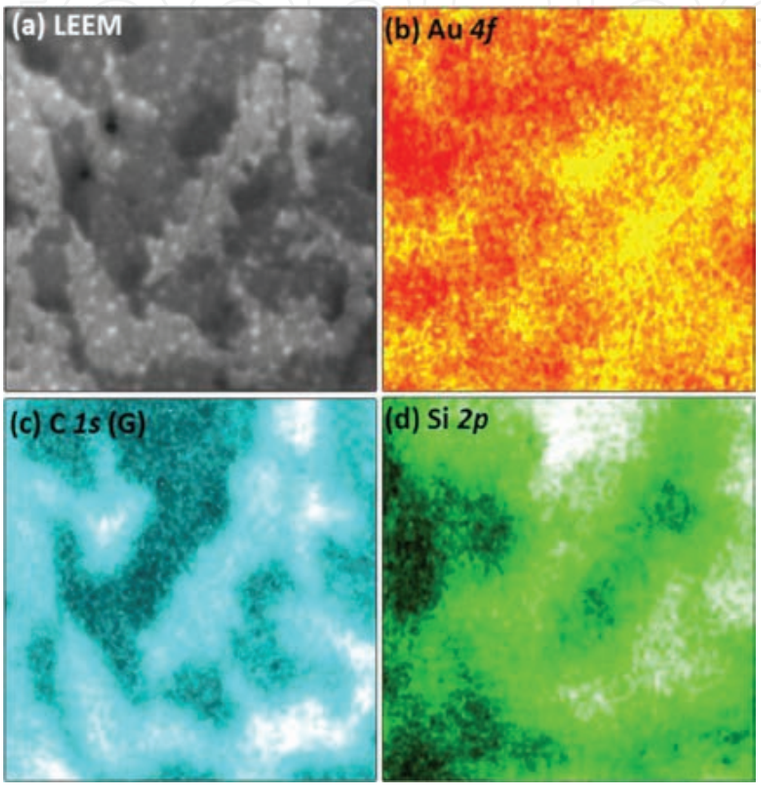

Figure 3. (a) LEEM image taken with an electron energy of 3.90 eV and (b–d) its corresponding XPEEM images recorded at the Au 4f, C 1s, and Si 2p core levels. The field of view is 0.80 μm wide. (b) Au 4f XPEEM image taken at a binding energy of 84.15 eV with hν = 200 eV. The highest (lowest) contrast is presented by the yellow (red) color. (c) C 1s XPEEM image taken at a binding energy of 284.60 eV with hν = 200 eV. The highest (lowest) contrast is presented by the white (black) color. (d) Si 2p XPEEM image, taken at a binding energy of 101.75 eV with hν = 200 eV. The highest (lowest) contrast is presented by the white (black) color.

In the following, we focus on the sample S1, corresponding to **Figure 2a** and **b**. In order to investigate the chemical properties of the sample after Au deposition, we have performed XPEEM measurements [29] at the C 1s, Au 4f, and Si 2p core levels (**Figure 3b–d**). **Figure 3a** displays a LEEM image of the sample after gold deposition, at electron energy of 3.90 eV. This image is a zoom of **Figure 2b**, marked by a dashed yellow square. **Figure 3c** is an XPEEM image at the C 1s core level, recorded at a binding energy (BE) of 284.60 eV. The BE is chosen to correspond to the maximum of the C 1s core level emission from the graphene layers. Therefore, the brightest (darkest) areas correspond to the graphene (substrate) layer. Regarding the Si 2p image, for which the maximum of intensity is attributed to the SiC contribution, recorded at a BE of 101.75 eV (hν = 200 eV), one can observe that the contrast is inverted, in comparison

http://dx.doi.org/10.5772/64076

with the C 1s XPEEM image. Indeed, a lower Si signal is due to attenuation by the graphene layers; and the corresponding zones, on the C 1s image appear bright. We verified that these two images are in agreement with the graphene thickness, evaluated in LEEM (**Figure 3a**). The shapes of the domains observed in the LEEM image can be easily recognized in the C 1s and Si 2p maps. In addition to the C and Si distributions, **Figure 2b** displays an image of the Au 4f, recorded at 84.15 eV binding energy (hν = 200 eV). The Au 4f signal seems to be more intense at the buffer layer. The shape of the previous domains is not clearly recognizable anymore, meaning that the Au can be deposited or/and intercalated independently of the surface chemistry (substrate/graphene mono- or bilayer). The LEEM/XPEEM images do not allow a clear discrimination between whether the Au nanoclusters are intercalated between adjacent graphene layers or between the graphene and the buffer layer, or if they simply overlay on the surface. The STEM data presented below will help answering this question.

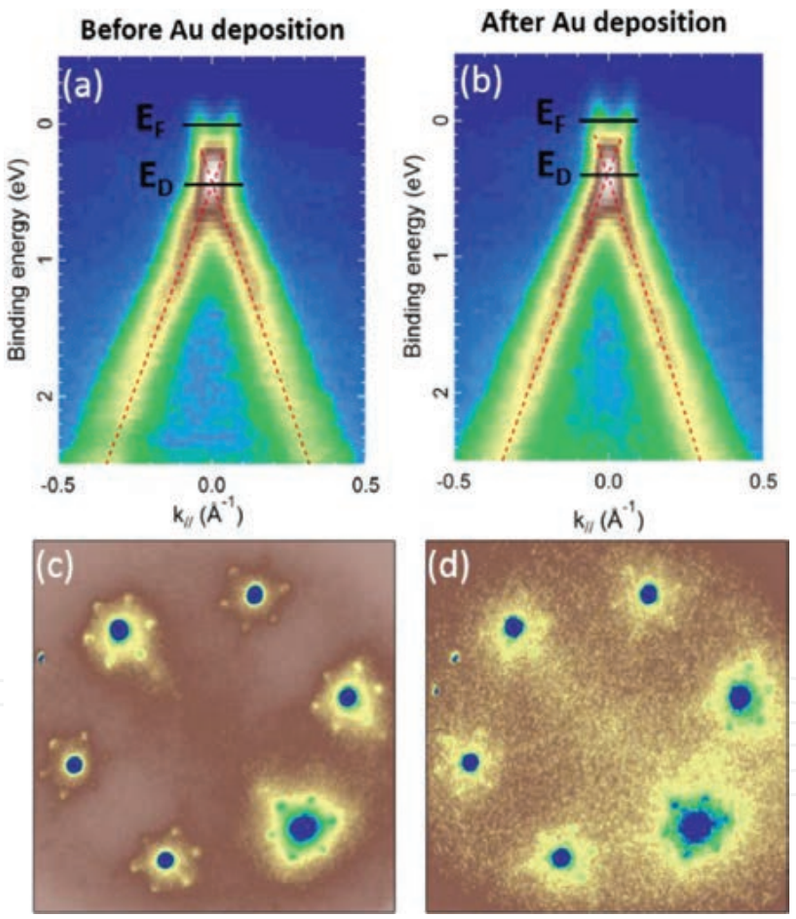

Figure 4. Top: band dispersions as a function of $k_{//}$ around the *K* point of the first Brillouin zone, obtained by μARPES at hν = 40 eV, performed before (a) and after (b) Au deposition. The Fermi level and the Dirac point are superimposed on the images. Bottom: 2D maps as a function of k_x and k_y, recorded for a binding energy of 0.15 eV, that is, close to the Fermi level, before (c) and after (d) gold deposition.

In order to investigate the effect of Au deposition on the electronic properties, we have performed local ARPES experiments (μARPES). **Figure 4** presents the μARPES maps, before

(**Figure 4a**) and after (**Figure 4b**) Au deposition, around the K point, perpendicular to the ΓKM direction. The 2D map of the unexposed graphene surface (**Figure 4a**) presents a shift of the Dirac point of 0.4 eV below the Fermi level. This energy shift ($\Delta E = E_D - E_F$) is nowadays well known in epitaxial graphene/SiC(0 0 0 1) [9, 17, 24] and is attributed to doping from the buffer layer [6, 7]. On the 2D μARPES map, recorded after Au deposition (**Figure 4b**), the energy difference between the Fermi level and the Dirac point is still 0.40 ± 0.02 eV. In our data, we do not observe a noticeable modulation of the Dirac point energy, contrary to what reported by Gierz et al. [21]. Nevertheless, we cannot exclude that a small shift of the Dirac point (below ~20 meV) has occurred. Moreover, Au deposition on SiC(0 0 0 1) results in p- or n-doping, depending either on the number of graphene layers, the strain at the Au/graphene or SiC/graphene interfaces [22], or the gold coverage [21]. In our case, we average the electronic information over the region that is slightly larger than that defined by the illumination, which includes both single and bilayer graphene. The local doping effect can therefore be averaged out in our data by the presence of areas with different electronic properties where Au induces p-doping and n-doping effect, respectively. However, we reckon that these antagonistic effects have to be insignificant for both cases as the Dirac cone does not get broader or split upon Au deposition.

The 2D maps of the first Brillouin zone, recorded for a BE of 0.25 eV, are presented in **Figure 4c** and **d**, close to the Fermi level, obtained before and after Au deposition, respectively. In the constant energy plots, six weak replicas of the π and π* states surrounding the primary states can be seen, as points around the upper spot (**Figure 4c**). Low-energy electron diffraction of graphene layers grown on the SiC substrate (not shown) displays a nearly commensurate superstructure with $(6\sqrt{3} \times 6\sqrt{3})R \times 30°$ unit cell with respect to the substrate because of the difference between the graphene lattice constant of 2.46 Å and that of SiC, 3.07 Å. The replicas of the π and π* states are brought about by scattering off this superstructure in a fashion similar to those in other incommensurate systems. The 2D image recorded after Au deposition (**Figure 4d**) shows that the superstructure around each K and K′ point persists. Even if the statistics are not as good as the one before Au adsorption, one can still clearly observe these satellites, which suggest that the Au deposition has not effectively decoupled the buffer layer from the substrate. The data in **Figure 4** demonstrate that the Au adsorption on this Gr/SiC(0 0 0 1) sample neither decouples the buffer layer from the substrate, nor alters its average doping.

In order to reach an atomic level characterization of the Au distribution we have performed sectional HR-TEM on the sample 2, after gold deposition. **Figure 5** shows TEM images of two distinct areas of the sample, recorded with a bright field (BF) and dark field mode (DF). These STEM images, allow accessing the crystallographic information. High-angle annular dark field (HAADF) contrast depends directly on the atomic number of the element: gold atoms appear very bright due to their high atomic number (so-called Z-contrast' imaging). The contrast of the graphene layer is very weak in the HAADF-STEM images due to its low atomic number (by comparison with the silicon). The graphene layer is easily visible in the bright field image (contrast of diffraction), as shown in **Figure 5b** and **e**.

http://dx.doi.org/10.5772/64076

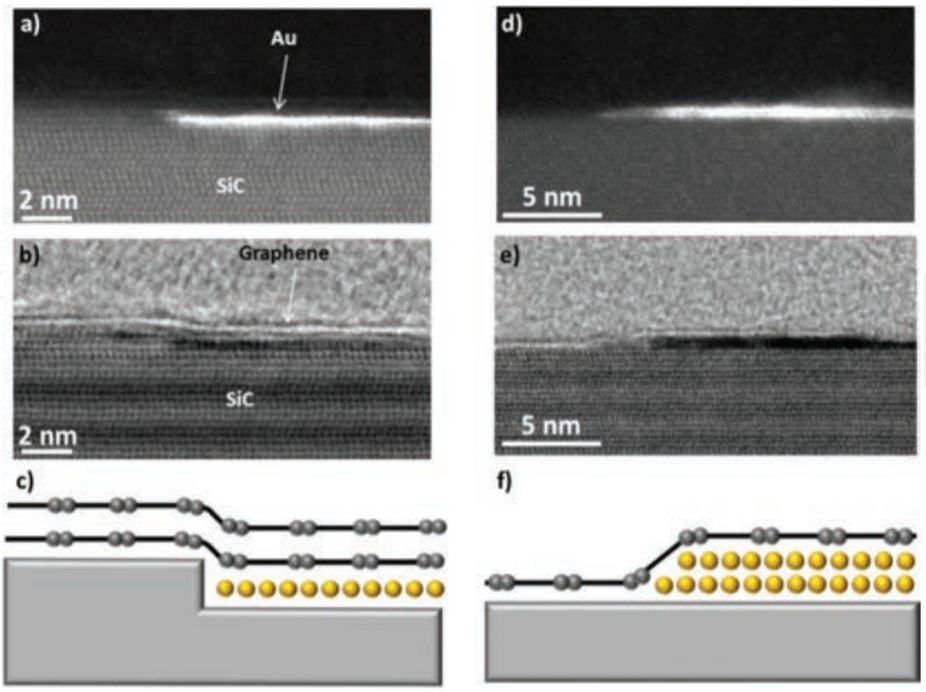

Figure 5. Cross-sectional aberration-corrected STEM images recorded in the high-angle annular dark field (HAADF) (a and d) and bright field (BF) (b and e) mode, respectively. HAADF contrast depends directly on the atomic number of the element: gold atoms appear very bright due to their high atomic number (so-called 'Z-contrast' imaging). The contrast of the graphene layer is very weak in the HAADF-STEM images due to its low atomic number (in comparison with the silicon). Layer graphene is easily visible in the bright field image (contrast of diffraction). The substrate, the Au, and graphene layers can clearly be observed. A scheme of the area is also represented. (d–f) DF and BF images with the associated scenarios, for another area of the surface. The substrate is represented by a gray square-shape. The Au and carbon atoms are represented by yellow and gray spheres.

On the DF images (**Figure 5a** and **d**), the bright contrast corresponds to the Au atoms. Moreover, the dark line above the crystalline substrate, observed on the DF image, is assigned to a graphene layer. For the first area (**Figure 5a** and **b**), combining the information extracted from the DF and BF images, respectively, we demonstrate that the Au atoms are located below the two graphene layers. These images also show that this Au insertion line stops at the step edge of the substrate, as presented in the sketch (**Figure 5c**). The BF image of the second area (**Figure 5d**) shows that two Au layers have been intercalated under a single graphene layer. Whether the graphene layer is continuous or not at the end of the Au step edge is not clear. One remaining question is how the Au penetrates into the sample. The Au atoms can penetrate the graphene layer through step edges or defects, as it has already been theoretically proposed in the case of the Si out-diffusion, on epitaxial graphene [30].

As different Au insertion mode have observed with the STEM with the HAADF imaging mode, a new set of images from another area, using once again the BF and DF modes, is presented **Figure 6**. The DF mode shows that two zones of the field of view contain Au atoms. The one on the left side shows that these atoms can pass through the graphene layer, as explained for **Figure 5**. However, the zone on the right side of the image presents a new scenario of Au adsorption. The Au atoms, as presented by the black dots of the BF, have penetrated into few layers of the substrate and a nanocluster has nucleated. The lateral size of this nanocluster can

be estimated to be ~5 nm. By scanning several areas of the surface, all of these three scenarios have been observed several times, confirming that the Au deposition on the graphene layer is not a uniform process.

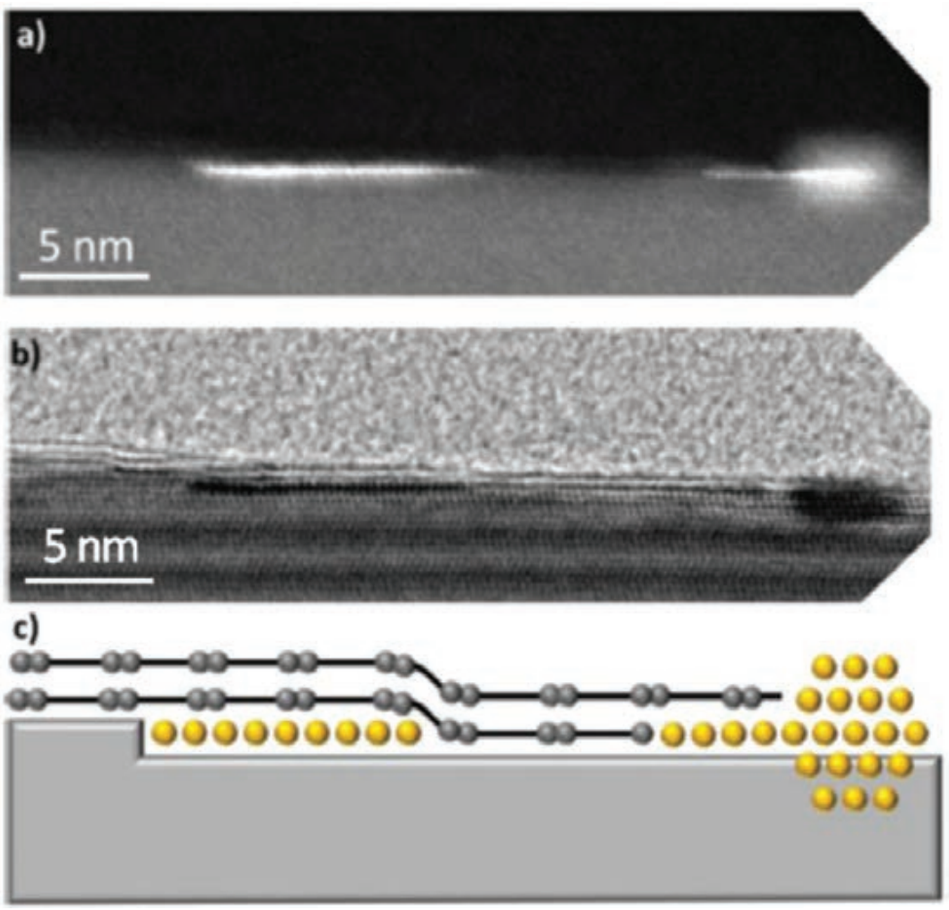

Figure 6. Cross-sectional STEM images recorded in the HAADF (top) and bright field (middle) mode, respectively. The substrate, the Au, and graphene layers can clearly be observed. A scheme of the area is also represented (bottom). The substrate is represented by a gray square shape. The Au and carbon atoms are represented by yellow and gray spheres.

The lateral distances between the gold atoms in the first layer are exactly the ones found for the silicon (or carbon) atoms of the SiC substrate underneath. Indeed, the distance measured between two adjacent Au atoms is 0.265 nm, while it is of 0.267 nm for two adjacent Si atoms in a (0 0 0 2) plane. These distances are obtained with the same value in measurements performed on numerous STEM images. The distance between two adjacent Au atoms in the second layer systematically decreases to 0.236 nm. Moreover, the distance between two adjacent gold layers is 0.255 nm, considering that the d_{0002} inter-reticular distance measured in the SiC substrate close to the surface is 0.266 nm. This value has to be compared to the experimental value of 0.252 nm [31] for the SiC bulk. Therefore, we can conclude that the strain in the SiC substrate beneath the surface is small, even when layer or nanoclusters of gold are observed.

The results observed in TEM and LEEM shows two main scenarios of gold migration when deposited on graphene/SiC(0 0 0 1). On the one hand, 1 or 2 ML of gold can intercalate between the substrate and the graphene layers. On the other hand, some gold atoms migrate inside the substrate to form nanoclusters. In the former case, this would lead to a change in the electronic properties, while it should not in the latter case. μ-ARPES measurements (**Figure 4**) do not present any noticeable changes. Before and after gold deposition, the Dirac point is at 0.40 eV below the Fermi level, for both cases. This equivalent doping can be explained by the fact that the gold mainly clusterizes and does not intercalate homogeneously under graphene layer. Therefore, the decoupling of the buffer layer, as observed by Gierz et al. [21], is not evidenced in our case.

4. Conclusions

In summary, we have demonstrated that the Au deposition on graphene epitaxially grown on SiC is an inhomogeneous process. The LEEM and XPEEM measurements have demonstrated that the Au nanoclusters nucleate all over the surface, independently of the surface chemistry (substrate, mono-, and bilayers of graphene). The STEM experiments have shown that the gold can diffuse under one or more graphene layers and can spread as one or two gold layers. Moreover, the gold mainly nucleates to form Au nanoclusters, which are spread all over the sample, independently of the surface chemistry. Therefore, the μARPES experiments have highlighted that the gold deposition does not induce a significant change in the electronic properties of this material and showed that the Fermi velocity of graphene remained intact in comparison with pristine graphene.

Author details

Claire Mathieu[1], Tevfik Onur Menteş[2], Emiliano Pallecchi[3], Andrea Locatelli[2], Gilles Patriarche[4], Rachid Belkhou[5] and Abdelkarim Ouerghi[4*]

*Address all correspondence to: abdelkarim.ouerghi@lpn.cnrs.fr

1 SPEC, CEA, CNRS, Paris-Saclay University, CEA Saclay, Gif-sur-Yvette Cedex, France

2 Elettra – Sincrotrone Trieste S.C.p.A., Basovizza, Trieste, Italy

3 Institut of Electronics, Microelectronics, and Nanotechnology (IEMN), Villeneuve d'Ascq Cedex, France

4 CNRS, Laboratory for Photonics and Nanostructures, Marcoussis, France

5 Synchrotron SOLEIL, Saint-Aubin, Gif-sur-Yvette Cedex, France

References

[1] Novoselov KS, Geim AK, Morozov SV, Jiang D, Zhang Y, Dubonos SV, Grigorieva IV, Firsov AA. Electric field effect in atomically thin carbon films. Science. 2004;306:666–669. doi:10.1126/science.1102896

[2] Berger C, Wu X, First PN, Conrad EH, Li X, Sprikle M, Hass J, Varchon F, Magaud L, Sadowski ML, Potemski M, Martinez G, de Heer WA. Dirac particles in epitaxial graphene films grown on SiC. Advances in Solid State Physics. 2008;47:145. doi: 10.1007/978-3-540-74325-5_12

[3] Virojanadara C, Syvajarvi M, Yakimova R, Johansson LI, Zakharov AA, Balasubramanian T. Homogeneous large-area graphene layer growth on 6H-SiC(0 0 0 1). Physical Review B. 2008;78:245403. doi:10.1103/PhysRevB.78.245403

[4] Sprinkle M, Ruan M, Hu Y, Hankinson J, Rubio-Roy M, Zhang B, Wu X, Berger C, de Heer WA. Nanoelectronics: nanoribbons on the edge. Nature Nanotechnology. 2010;5:698–699. doi:10.1038/nnano.2010.200

[5] Emtsev KV, Speck F, Seyller Th, Ley L, Riley JD. Interaction, growth and ordering of epitaxial graphene on SiC(0 0 0 1) surfaces: a comparative photoelectron spectroscopy study. Physical Review B. 2008;77:155303. doi:10.1103/PhysRevB.77.155303

[6] Ouerghi A, Marangolo M, Belkhou R, El Moussaoui S, Silly MG, Eddrief M, Largeau L, Portail M, Fain B, Sirotti F. Epitaxial graphene on 3C-SiC(1 1 1) pseudosubstrate: structural and electronic properties. Physical Review B. 2010;82:125445. doi:10.1103/PhysRevB.82.125445

[7] Varchon F, Feng R, Hass J, Li X, Ngoc Nguyen B, Naud C, Mallet P, Veuillen J-Y, Berger C, Conrad EH, Magaud L. Electronic structure of epitaxial graphene layers on SiC: effect of the substrate. Physical Review Letters. 2007;99:126805. doi:10.1103/PhysRevLett.99.126805

[8] Ouerghi A, Silly MG, Marangolo M, Mathieu C, Eddrief M, Picher M, Sirotti F, El Moussaoui S, Belkhou R. Large-area and high-quality epitaxial graphene on off-axis SiC wafers. ACS Nano. 2012;6:6075–6082. doi:10.1021/nn301152p

[9] Coletti C, Riedl C, Lee DS, Krauss B, Patthey L, von Klitzing K, Smet JH, Starke U. Charge neutrality and band-gap tuning of epitaxial graphene on SiC by molecular doping. Physical Review B. 2010;81:235401. doi:10.1103/PhysRevB.81.235401

[10] Zhou SY, Siegel DA, Fedorov AV, Lanzara A. Metal to insulator transition in epitaxial graphene induced by molecular doping. Physical Review Letters. 2008;101:086402. doi: 10.1103/PhysRevLett.101.086402

[11] Gierz I, Riedl C, Starke U, Ast CR, Kern K. Atomic hole doping of graphene. Nano Letters. 2008;8:4603–4607. doi:10.1021/nl802996s

[12] Emtsev KV, Zakharov AA, Coletti C, Forti S, Starke U. Ambipolar doping in quasifree epitaxial graphene on SiC(0 0 0 1) controlled by Ge intercaltion. Physical Review B. 2011;84:125423. doi:10.1103/PhysRevB.84.125423

[13] Walter AL, Jeon K-J, Bostwick A, Speck F, Ostler M, Seyller T, Moreschini L, Kim YS, Chang YJ, Horn K, Rotenberg E. Highly p-doped epitaxial graphene obtained by fluorine intercalation. Applied Physics Letters. 2011;98:184102. doi:10.1063/1.3586256

[14] Virojanadara C, Watcharinyanon S, Zakharov AA, Johansson LI. Epitaxial graphene on 6H-SiC and Li intercalation. Physical Review B. 2010;82:205402. doi:10.1103/PhysRevB.82.205402

[15] Virojanadara C, Zakharov AA, Watcharinyanon S, Yakimova R, Johansson LI. A low-energy electron microscopy and X-ray photo-emission electron microscopy study of Li intercalated into graphene on SiC(0 0 0 1). New Journal of Physics. 2010;12:125015. doi: 10.1088/1367-2630/12/12/125015

[16] Riedl C, Coletti C, Iwasaki T, Zakharov AA, Starke U. Quasi-free_standing epitaxial graphene on SiC obtained by hydrogen intercalation. Physical Review Letters. 2009;103:246804. doi:10.1103/PhysRevLett.103.246804

[17] Mathieu C, Lalmi B, Mentes TO, Locatelli A, Latil S, Belkhou R, Ouerghi A. Effect of oxygen adsorption on the local properties of epitaxial graphene on SiC(0 0 0 1). Physical Review B. 2012;86:035435. doi:10.1103/PhysRevB.86.035435

[18] Varykhalov A, Scholz MR, Kim TK, Rader O. Effect of noble-metal contacts on doping and band gap of graphene. Physical Review B. 2010;82:121101. doi:10.1103/PhysRevB.82.121101

[19] Nair MN, Cranney M, Vonau F, Aubel D, Le Fevre P, Tejeda A, Bertran F, Taleb-Ibrahimi A, Simon L. High van Hove singularity extension and Fermi velocity increase in epitaxial graphene functionalized by intercalated gold clusters. Physical Review B. 2012;85:245421. doi:10.1103/PhysRevB.85.245421

[20] Gao T, Gao Y, Chang C, Chen Y, Liu M, Xie S, He K, Ma X, Zhang Y, Liu Z. Atomic-scale morphology and electronic structure of manganese atomic layers underneath epitaxial graphene on SiC(0 0 0 1). ACS Nano. 2012;6(8):6562–6568. doi:10.1021/nn302303n

[21] Gierz I, Suzuki T, Weitz RT, Lee DS, Krauss B, Riedl C, Starke U, Höchst H, Smet JH, Ast CR, Kern K. Electronic decoupling of an epitaxial graphene monolayer by gold intercalation. Physical Review B. 2010;81:235408. doi:10.1103/PhysRevB.81.235408

[22] Chuang F-C, Lin W-H, Huang Z-Q, Hsu C-H, Kuo C-C, Ozolins V, Yeh V. Electronic structures of an epitaxial graphene monolayer on SiC(0 0 0 1) after gold intercalation: a first-principles study. Nanotechnology. 2011;22:275704. doi: 10.1088/0957-4484/22/27/275704

[23] Premlal B, Cranney M, Vonau F, Aubel D, Casterman D, De Souza MM, Simon L. Surface intercalation of gold underneath a graphene monolayer on SiC(0 0 0 1) studied

by scanning tunneling microscopy and spectroscopy. Applied Physics Letters. 2009;94:263115. doi:10.1063/1.3168502

[24] Locatelli A, Knox KR, Cvetko D, Mentes TO, Nino MA, Wang S, Yilmaz MB, Kim P, Osgood RM, Jr, Morgante A. Corrugation in exfoliated graphene: an electron microscopy and diffraction study. ACS Nano. 2010;4:4879. doi:10.1021/nn101116n

[25] Locatelli A, Aballe L, Mentes TO, Kiskinova M, Bauer E. Photoemission electron microscopy with chemical sensitivity: SPELEEM methods and applications. Surface and Interface Analysis. 2006;38:1554–1557. doi:10.1002/sia.2424

[26] Ouerghi A, Ridene M, Balan A, Belkhou R, Barbier A, Gogneau N, Portail M, Michon A, Latil S, Jegou P, Shukla A. Sharp interface in epitaxial graphene layers on 3C-SiC(1 0 0)/Si(1 0 0) wafers. Physical Review B. 2011;85:205429. doi:10.1103/PhysRevB.83.205429

[27] Pallecchi E, Ridene M, Kazazis D, Mathieu C, Schopfer F, Poirier W, Mailly D, Ouerghi A. Observation of the quantum Hall effect in epitaxial graphene on SiC(0 0 0 1) with oxygen adsorption. Applied Physics Letters. 2012;100:253109. doi:10.1063/1.479824

[28] Feenstra RM, Srivastava N, Gao Q, Widom M, Diaconescu B, Ohta T, Kellogg GL, Robinson JT, Vlassiouk IV. Low-energy electron reflectivity from graphene. Physical Review B. 2013;87:041406(R). doi:10.1103/PhysRevB.87.041406

[29] Knox KR, Locatelli A, Yilmaz MB, Cvetko D, Mentes TO, Nino MA, Kim P, Morgante A, Osgood RM, Jr. Making angle-resolved photoemission measurements on corrugated monolayer crystals: suspended exfoliated single-crystal graphene. Physical Review B. 2011;84:115401. doi:10.1103/PhysRevB.84.115401

[30] Sun GF, Liu Y, Rhim SH, Jia JF, Xue QK, Weinert M, Li L. Si diffusion path for pit-free graphene growth on SiC(0 0 0 1). Physical Review B. 2011;84:195455. doi:10.1103/PhysRevB.84.195455

[31] Nakagawa H, Tanaka S, Suemune I. Self_ordering of nanofacets on vicinal SiC surfaces. Physical Review Letters. 2003;91:226107. doi:10.1103/PhysRevLett.91.226107